PHILOSOPHICAL TRANSACTIONS A

Phil. Trans. R. Soc. A.

doi:10.1098/not yet assigned

Predicting Concurrent Structural Mechanical Mechanisms During Microstructure Evolution

P Soar[1], A Kao[1*], N Shevchenko[2], S Eckert[2], G Djambazov[1] and K Pericleous[1]

[1]*Centre for Numerical Modelling and Process Analysis, University of Greenwich, Old Royal Naval College, Park Row, London, SE10 9LS, UK*

[2]*Helmholtz-Zentrum Dresden-Rossendorf, Institute of Fluid Dynamics, Bautzner Landstrasse 400, 01328 Dresden, Germany*

Keywords: dendrite deformation; crystallographic orientation; microstructure solidification; numerical modelling; structural mechanics

Summary

The interdependence between structural mechanics and microstructure solidification has been widely observed experimentally as a factor leading to undesirable macroscopic properties and casting defects. Despite this, numerical modelling of microstructure solidification often neglects this interaction and is therefore unable to predict key mechanisms such as the development of misoriented grains. This paper presents a numerical method coupling a Finite Volume Structural Mechanics Solver to a Cellular Automata Solidification Solver, where gravity or pressure-driven displacements alter the local orientation and thereby growth behaviour of the solidifying dendrites. Solutions obtained using this model are presented which show fundamental behaviours observed in experiments. The results show that small, localised deformations can lead to significant changes in crystallographic orientation of a dendrite and ultimately affect the overall microstructure development.

1. Introduction

Structural mechanics is one of many factors that can significantly impact the microstructural development of metal alloys during casting. The composition of the dendrites formed during the solidification process dictate the macroscopic material properties of any solidified parts. Consequently, gaining greater understanding and control over the solidification process can aid the processing of alloys to achieve more desirable properties, for example eliminating defects and structural inhomogeneities occurring in the Twin Roll Casting process [1]. However, the interdependent nature of the relationship between the solidification process and structural mechanics is a complex one with many potential sources of forces which can cause observable deformations to

*Andrew Kao (A.Kao@gre.ac.uk).

†Present address: Centre for Numerical Modelling and Process Analysis, University of Greenwich, Old Royal Naval College, Park Row, London SE10 9LS, UK

manifest. When structural mechanics causes movement in the microstructure it will necessarily alter the solidification behaviour to account for local displacement, with this altered behaviour feeding back to cause further mechanical changes. In extreme cases this can lead to dendrite arms deforming or even fracturing [2,3], leading to casting defects such as stray grains [4,5] and slivers [6,7] which negatively impact the material properties of the cast part, potentially leading to them being discarded.

A deforming dendrite will also likely incur a change in crystallographic orientation, itself an important factor in determining the final material properties [8]. This change in orientation will alter the preferred growth direction of the dendrite, which can sometimes have a larger impact on the dendritic system than the initial deformation which caused the misorientation.

These orientation dominated cases can arise from large, localised changes where the arm will continue along the new orientation with no further significant misorientation [9,10] as well as from long dendrite arms gradually accumulating misorientations for the duration of their development, often becoming significantly different to the orientation they were seeded with [11–13].

More commonly, structural mechanics is only applied at the end to post process fully solidified structures [14,15]. Time dependent effects have been considered, but generally only at different discrete levels of development [16,17] only considering temperature driven mechanical interactions and operating at a macroscopic scale where, if not overlooked entirely, the composition of the microstructure is modelled indirectly [18].

A truly coupled approach considering the interdependence of solidification with structural mechanics was developed by Yamaguchi and Beckermann [19,20] which combined a phase field solidification model with the finite element method while also considering the crystallographic orientation. However, this approach was for a pure substance with limited ways to apply force to the structure, with the authors identifying several required improvements before this approach could be applied to alloys.

In this work, microstructural evolution is intimately coupled to the effect of structural mechanical forces, where localised deformations lead to changes in the crystallographic orientation. Over time, the accumulation of misorientation can become significant and alter the behaviour of key mechanisms that can be influenced by orientation, such as competitive growth [21,22] and side branching [23].

The results presented in this paper will be focussed on demonstrating the fundamental behaviour of structural mechanical forces acting on dendrites to cause accumulating misorientations as they grow. This leads to a contrasting microstructure to cases which fail to account for these forces.

2. Numerical Method

(a) Solidification

A finite difference decentred octahedral Cellular Automata (CA) method based on the μMatIC code [24–27] is used to resolve the evolution of the alloy microstructure. Phase change and the partitioning of solute is governed by

$$C_l(1-k)\frac{\partial \phi_s}{\partial t} = -\nabla \cdot (D_e \nabla C_l) + [1-(1-k)\phi_s]\frac{\partial C_l}{\partial t} \quad (1)$$

and diffusive transport by

$$\frac{\partial C_e}{\partial t} = \nabla \cdot (\mathrm{D_e} \nabla \mathrm{C_l}) \quad (2)$$

where the equivalent concentration $C_e = (1-\phi_s)C_l + \phi_s C_s$, C_l is the liquid concentration, C_s is solid concentration, $k = C_l/C_s$ is the partition coefficient, $0 \leq \phi_s \leq 1$ is the solid fraction, D_e is the mass diffusivity and t is time. The equilibrium temperature T_i is given by

$$T_i = T_0 + m_l(C_l - C_0) \quad (3)$$

where m_l is the liquid slope, C_0 is the initial concentration and T_0 is the liquidus temperature at C_0. This method has been further developed by the authors in the microstructure modelling framework TESA [28,29] to solve complex multi-physics phenomena, capable of running large scale microstructural simulations in parallel.

(b) Structural Mechanics

The material model solves the Linear Elasticity equations to describe the structural mechanical behaviour. This necessitates the following assumptions: deformations are 'small', a linear relationship exists between the stress and strain, only elastic deformation and plain strain when resolving in two dimensions. Attempts at both modelling [15,20] and interpretations of experimental results [2,11,13,30] use cantilever beams as an analogy to the behaviour of columnar dendrites, recognising the beam theory is in itself a further simplification of Linear Elasticity. These simplifying assumptions are applicable to problems where the deformation per unit time is small relative to solidification velocity and the accumulation of misorientation dominates physical movement caused by deformation.

Considering these assumptions, a bespoke Finite Volume Structural Mechanics Solver (FVSMS) was developed that can be directly coupled with the CA method in the TESA framework. The FVSMS uses a

staggered mesh, with displacements stored at cell faces. While more often applied to Computational Fluid Dynamics problems, there have been many examples of the finite volume method being used for Structural Mechanics where a comparable level of accuracy to the more commonly utilised Finite Element Method is attained [31–33].

This solver was developed to solve the pair of partial differential equations obtained by using Hooke's law to transform the stationary solution to the linear elasticity equations into a displacement formulation given by:

$$(2\mu + \lambda)\frac{\partial^2 u_x}{\partial x^2} + (\lambda + \mu)\frac{\partial^2 u_y}{\partial x \partial y} + \mu\frac{\partial^2 u_x}{\partial y^2} + F_x = 0 \tag{4}$$

$$(2\mu + \lambda)\frac{\partial^2 u_y}{\partial y^2} + (\lambda + \mu)\frac{\partial^2 u_x}{\partial x \partial y} + \mu\frac{\partial^2 u_y}{\partial x^2} + F_y = 0 \tag{5}$$

where u_x and u_y are the displacements in the x and y direction, F_x and F_y are the corresponding body forces, μ and λ are the Lamé constants,

$$\lambda = \frac{\nu E}{(1+\nu)(1-2\nu)} \quad \text{and} \quad \mu = \frac{E}{2(1+\nu)}, \tag{6}$$

where E and ν are respectively the Young's Modulus and Poisson's ratio of the material.

Structural mechanics is treated as a quasi-stationary process, where rather than keeping track of the total displacement in the structure, only the displacements which have occurred since the prior call of the solver is calculated. This requires the body forces F_x and F_y applied in each volume to behave transiently, so that rather than the total force, these use instead the change in force when compared to the prior time step. Both the FVSMS and CA method use fixed Cartesian grids, such that material properties and stored variables align.

The FVSMS has been designed to handle structures with variable material properties, which has been exploited to avoid the potential complications that could arise from using a body fitted Finite Element mesh, where progressing solidification may necessitate remeshing. This was achieved by also solving structural mechanics in a region surrounding the structure, using a functionally zero Young's Modulus value for the liquid, a million times smaller than the value used inside the solid. This assumes that a material with a sufficiently small Young's Modulus approximates liquid behaviour and offers no significant resistance to the movement of the solid structure. Note, that we could in fact solve fluid flow on the same mesh, simply using a change of variables, with velocities replacing displacements stored at cell faces, a planned future extension.

The structural mechanics problem can then be defined by the local material properties and application of force within this domain, which are themselves defined by the solid fraction and concentration values

provided for each volume by the CA method. A similar method has been applied by Uehara, Fukui and Ohno [34], using a Finite Element Method with a fixed mesh to avoid the remeshing issue described, updating the material properties at the nodes as the domain solidifies.

(c) Cell Orientation and Model Coupling

The code allows for the crystallographic orientation of dendrites to vary spatially, so that each cell comprising the structure has a local crystallographic orientation θ inherited from a parent cell and which can be updated using local displacements obtained from the FVSMS. This allows the primary and secondary arms of dendrites to potentially develop significantly different orientations as the microstructure develops. The displacements obtained at the faces of the volume can be used to form an arc by summing the displacements, a schematic of this is given in figure 1. This arc corresponds to an extrinsic rotation about the axis defined as

$$d\theta = \frac{1}{2\Delta \mathrm{x}}(v_e - v_w - u_n + u_s) \approx \frac{1}{2}\left(\frac{\partial v}{\partial \mathrm{x}} - \frac{\partial u}{\partial \mathrm{y}}\right) \tag{7}$$

where v_e and v_w are the displacements in y at the east and west face of the cell and u_n and u_s are the displacements in x at the north and south faces of the cell. An important aspect of this formulation is that the rotation is functionally dependent on the derivative of the displacements and not the magnitude. Therefore, in cases with small displacements, but relatively large, localised gradients the evolution of the structure will be dominated by changes to the crystallographic orientation as opposed to the physical movement. The obtained $d\theta$ values are then added to the existing orientation profile of the structure, which will then dictate the development of the CA method until the next time structural mechanics is called.

In summary, over a transient solution step, the CA method calculates the evolution of the microstructure and from this, changes to material properties and body forces. These are then passed to the FVSMS which calculates deformations that are used to update the local crystallographic orientations. The CA method is then called again and the solution progresses.

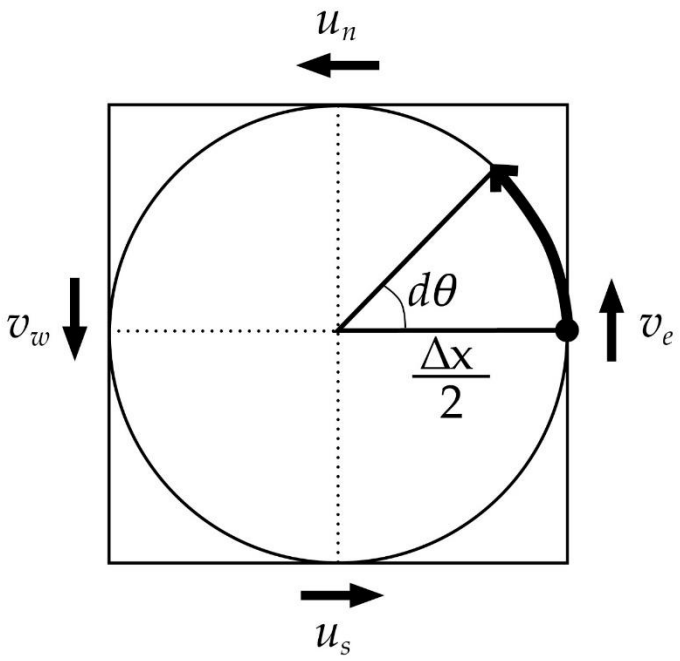

Figure 1. Schematic showing how the arc used to calculate $d\theta$ is constructed.

(d) Experimental Setup

The experiment presented in this paper examines solidification in a differentially heated cavity with a temperature gradient perpendicular to gravity. This was conducted in a Hele-Shaw cell made of quartz with a liquid metal volume of 29 × 29 × 0.15 mm^3 composed of low melting point hypereutectic Ga-25 wt%In alloy prepared from gallium and indium of 99.99% purity. A temperature gradient of 1.2 $\pm$0.2 K/mm with a cooling rate of 0.01 K/s was applied across the cell by mounting two pairs of Peltier elements as a heater and a cooler on the right and left edges of the cell, respectively.

In situ and real time observations of the solidification process through a rectangular observation window of about 13 × 17 mm^2 was attained by mounting the solidification setup on a three-axis translation stage between a microfocus X-ray source and X–ray detector. This is similar in setup to the experiments presented in a paper by Kao *et al*. [28], which can provide further detail on the experimental setup.

(e) Modelling Setup

The two-dimensional computational domain is 64 mm × 16 mm in size divided by square cells with a 10 μm side. The west wall is fixed with zero displacement. The temperature is defined by assuming a constant

temperature gradient of 1 K/mm in x, cooling at a constant rate of 1 K/s with the west wall initially at a small undercooling, 5 K below the liquidus temperature. Nuclei that initiate solidification are seeded on this wall and solidification then proceeds predominately from the west to the east. The north and south boundaries are periodic such that the system could be considered to represent a section of a large sample. As solidification proceeds and solute is rejected at the interface, a density difference between the solid and liquid forms. In the cases considered, the dendrites are Indium enriched and hence have a higher density than the liquid. This manifests as a body force, where the density difference is calculated from the concentration in the solid compared to the interfacial equilibrium concentration.

$$\mathrm{F_y} = \Delta\rho \mathrm{g} = \frac{\mathrm{g}}{100}\left((\mathrm{C}_e\rho_{Ga} + (1 - C_e)\rho_{In}) - (C_i\rho_{Ga} + (1 - C_i)\rho_{In})\right) \quad (8)$$

In this work the gravitational acceleration, g, is assumed to be three times larger than terrestrial conditions. This super gravity condition makes it easier to highlight the fundamental behaviour of the coupled system. It can be assumed that many observed structural mechanical effects in experiments are a consequence of additional forces, such as hydrodynamic pressures and not just the weight of the dendrites, otherwise strong structural mechanical effects would be consistently observed in all alloys that exhibit density variations.

Timesteps in the weakly coupled framework of the solvers were chosen to provide a balance of speed and accuracy between the solvers, with the results of timestep dependence tests leading to the CA method being solved every 5ms and the structural mechanics every 2.5s.

At the microscale the temperature variations are small, i.e. ~0.1 K over 100 microns and so the effect of thermal expansion has been neglected and material properties are temperature independent; chosen to be characteristic of those close to the melting temperature.

The value being used for the Young's Modulus of the dendrite was the lower bound calculation for a semi solid alloy within the eutectic temperature region, which was determined from the compressibility of constrained liquid Indium and Gallium [35] which is significantly different to the nominal value used for the Young's Modulus of the free liquid regions being solved. However, there was no evidence of similar variation in Poisson's ratio for semi solid metals, so a constant value matching the solidified alloy was used.

The material properties being used in this experiment model representing Ga-25 wt%In are provided in table 1.

Table 1. Material property values used for simulation.

Property	Variable	Value	Unit
Density Ga	ρ_{Ga}	6095	kg m−3
Density In	ρ_{In}	7020	kg m−3
Young's Modulus	E	30	MPa
Poisson's Ratio	ν	0.3	-
Liquidus slope	m_l	-2.9375	K %wt.$^{-1}$
Partition Coefficient	k	0.5	-
Liquid Mass diffusivity	D_l	2×10^{-9}	m^2 s^{-1}
Solid Mass diffusivity	D_s	1×10^{-12}	m^2 s^{-1}

3. Results and Discussion

The first case to be discussed concerns experimental results of the Ga-25 wt%In system shown in figure 2, where examples of dendrites becoming misoriented throughout the sample can be observed transiently. In figure 2(a) at an early point during the experiment, the dendrites begin with an orientation of around 20 degrees which does not seem to have significantly changed as they have grown. Figure 2(b) shows the sample at the conclusion of the experiment, where despite still clearly having an initial orientation of around 20 degrees by the base of the dendrite arms, the orientation at the tips has become closer to 10 degrees.

The dendrites are denser than the liquid and generally exhibit misorientations causing growth to deflect downwards toward the direction of gravity. However, the system is quite complex with strong fluid flow due to buoyancy effects from the low-density Gallium [28]. This would alter the distribution of solutes, changing the solidification behaviour along with the corresponding body forces obtained from the density changes. These effects may also cause significant remelting to occur, changing the thickness of the dendrite and consequently making it more susceptible to bending. Furthermore, the inter-dendritic flow present in the experiment could introduce significant forces from hydrodynamic pressures which may either reinforce or oppose the gravitational effects. Nevertheless, for the most part, this case highlights that many of the dendrites' crystallographic orientation is a consequence of continuous accumulation of small misorientations rather than singular large misorientation or noticeable large deformations.

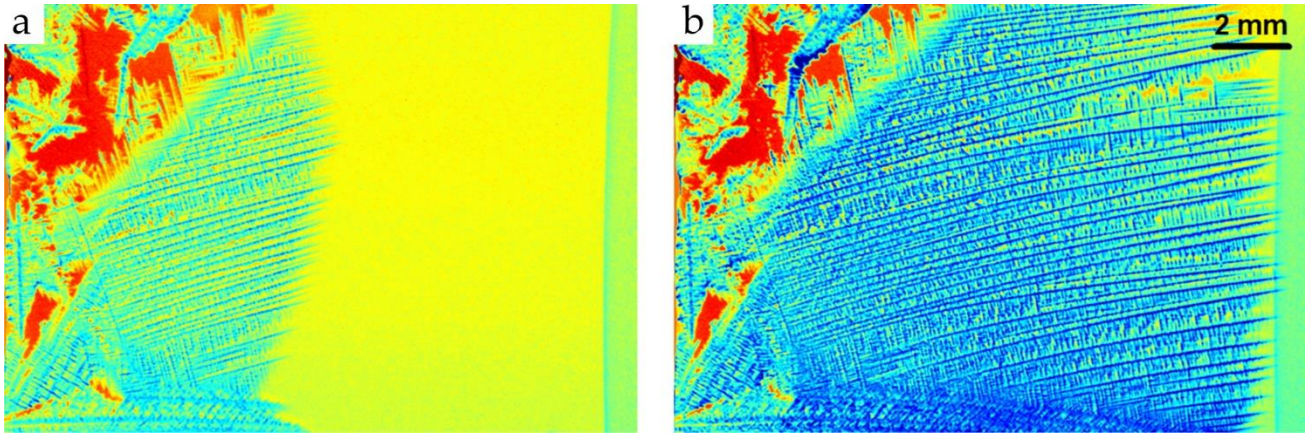

Figure 2. Experimental results showing the transient accumulation of misorientation during solidification of Ga-25 wt%In.

Numerical modelling results representative of the experimental conditions are given in figure 3. Figure 3(a-d) shows the transient evolution of the dendrites, figure 3(e) accumulated misorientation, figure 3(f) total v displacement, figure 3(g) the Von Mises stress and figure 3(h) the case with no applied force. In figure 3(a) the small size of the structure is causing no noticeable misorientation. In figure 3(b) there is now some visible misorientation, although still just over one degree at the tips of the arms. In figure 3(c), the orientations have accumulated to the point where they are starting to significantly affect the growth angle, getting close to entirely counteracting the starting orientation of 20°. By the final step in figure 3(d), the orientations have accumulated to such an extent the dendrite orientation at the tip has now entirely reversed the starting orientation, with the tip starting to bend in the opposing direction. This matches the general transient behaviour observed in in figure 2, with the misorientation growing as the dendrites increase in mass.

The total misorientation is given in figure 3(e), showing the local change in orientation occurring throughout the microstructure relative to the initial seeded orientation of 20°. It can be observed that the primary arms of the dendrites have started acting as a cohesive group, with similar orientations at the tip and along most of their arms. It can also be observed that the interaction of the secondaries can cause significant local misorientation, with many secondaries having noticeably higher or lower misorientation that the primary arm they initially shared an orientation with. The largest misorientations are toward the end of the dendrite, bending more as they grow longer. Figure 3(f) shows the accumulated v displacements within the dendritic structure, with the u displacements being omitted due to the dominance of v displacements in this scenario. The highest

deformation can be found somewhere in the centre of the dendrites, fading out towards the tip and root. Whilst potentially seeming counter intuitive, attaining the largest accumulated deformation in the structure requires a balance between the magnitude of the individual deformations against the total accumulated deformation. This condition is generally met in the centre of the dendrite as the tip has only experienced few deformations even if their magnitude is relatively large, while the root has conversely experienced many deformation events of a relatively small magnitude.

Figure 3(g) shows the Von Mises stress calculated from the accumulated displacements within the microstructure. These demonstrate two main regions where significant mechanical stresses accumulate: at pivot points for the bending primary arms where they are attached to a fixed point or a relatively more stable region of the microstructure; or where the primary arms find their attempted deformation constrained by the interaction of secondaries impinging upon each other.

Finally, figure 3(h) shows the contrasting behaviour of solidification without any applied force, where the crystallographic orientation remains unchanged. In the case with the applied force the maximum total v displacement is 4.5 mm. By comparing the tip of the primary dendrite arm to the case with no force and therefore no orientation change, the tip is approximately 13 mm lower than would have been expected with no structural mechanics being applied. Given that the final tip location has moved around three times the distance that could be explained purely by deformation, this observation supports the assumption that in many cases, including the one considered, orientation can be the dominant mechanism as opposed to direct deformation.

Figure 4 shows the last case where the parameters are identical to the previous case with the exception that one of the dendrites is assumed to have zero deformation. This represents the situation where the dendrite could have fused to or be constrained by some imperfection in the thin sample wall. With periodic conditions still applied, the case represents solidification of both converging and diverging grains due to structural mechanics. On the convergent side the bending dendrite is outcompeted by the non-misoriented grain and similarly on the divergent side the secondaries of the non-misoriented grain outcompete the misoriented grain. In this case the misoriented grain becomes stunted; however, grain competition is a complex process with dependencies on orientation, thermal conditions, spatial conditions and as explored here structural mechanical forces. Such behaviour of divergent and convergent grains can be seen in the experimental example in figure 2. Under more favourable conditions the misoriented grain could win the competition leading to the formation of a large stray grain.

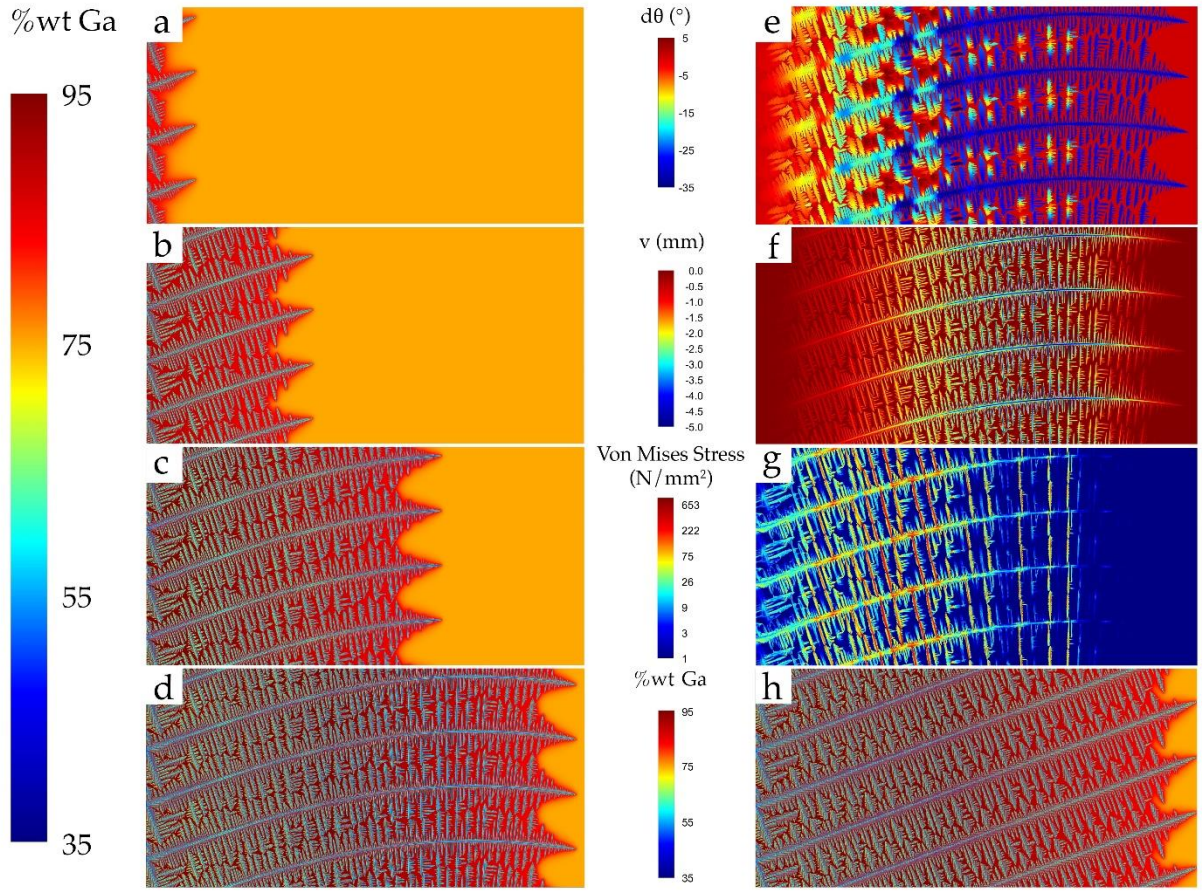

Figure 3. Numerical results (a-g) with an applied force and (h) without a force. (a-d) Transient evolution of the misorientating dendrites. (e) Misorientation. (f) Total v displacement (g) Von Mises stress. (h) Case with no applied force.

Figure 4. (a) Numerical results with converging grains. (b) Highlighted grains.

4. Conclusion and future work

The application of a local orientation framework allowed the FVSMS and CA method to be coupled into a microscale numerical model. This has predicted fundamental mechanisms of accumulated misorientations causing significant changes to microstructural development, capturing observed experimental behaviours that would not have been possible with existing models. Numerical results were obtained from solidifying the systems of dendrites with identical initial conditions under three scenarios: where no Structural Mechanical effects were considered, under supergravity and where a single grain was fixed. This was compared with an experiment conducted on a thin sample Ga-25 wt%In alloy, where the fundamental behaviour of dendrites becoming gradually misoriented across the length of the sample could be observed acting in an analogous manner to the modelling scenarios considering gravity. This demonstrates a clear structural mechanical impact on the interaction of secondary arms, primary arm spacing as well as the final crystallographic orientation of the dendrites. The Von Mises Stress inside the microstructure was also calculated to allow regions of high stress caused by these structural effects to be identified. These comparisons demonstrate there is potential for a significant impact to the accuracy of any microstructure solidification modelling which neglects the impact of structural mechanics.

With this fundamental behaviour successfully implemented, there are many avenues of future study. This includes extending the method to account for non-linear behaviour, for example plastic deformations and to account for large physical movements. Another key route is to include fluid flow which will change the distribution of the solute and potentially impart further forces on the growing structure. These will allow numerical simulations to capture a wider range of behaviours seen in experimental results, providing further insights into fundamental mechanisms linked to structural mechanics.

Additional Information

Data Accessibility
The datasets supporting this article have been uploaded to the University of Greenwich's repository, available from gala.gre.ac.uk.

Authors' Contributions
P.S. carried out the numerical simulations and analysis, developed the code and coupling, and drafted the manuscript. A.K. carried out analysis and drafted the manuscript. N.S. and S.E conducted the experiments and analysis. G.D. and K.P. drafted the manuscript. All authors read and approved the manuscript.

Competing Interests
The author(s) declare that they have no competing interests

Funding Statement
P.S. gratefully acknowledges the financial assistance offered by the University of Greenwich VC scholarship for his PhD studies.

References

1. Westengen H, Nes K. 2016 The occurrence of structure inhomogeneities and defects in as cast strip. In *Essential Readings in Light Metals*, pp. 972–980. Springer, Cham. (doi:https://doi.org/10.1007/978-3-319-48228-6_123)
2. Reinhart G, Nguyen-Thi H, Mangelinck-Noël N, Baruchel J, Billia B. 2014 In situ investigation of dendrite deformation during upward solidification of Al-7wt.%Si. *Jom* **66**, 1408–1414. (doi:10.1007/s11837-014-1030-z)
3. Reinhart G *et al.* 2008 In-situ and real-time analysis of the formation of strains and microstructure defects during solidification of Al-3.5 Wt Pct Ni alloys. *Metall. Mater. Trans. A Phys. Metall. Mater. Sci.* **39 A**, 865–874. (doi:10.1007/s11661-007-9449-2)
4. Yang C, Liu L, Zhao X, Zhang J, Sun D, Fu H. 2014 Formation of stray grains during directional solidification of a superalloy AM3. *Appl. Phys. A Mater. Sci. Process.* **114**, 979–983. (doi:10.1007/s00339-013-8046-z)
5. Zhou Y. 2011 Formation of stray grains during directional solidification of a nickel-based superalloy. *Scr. Mater.* **65**, 281–284. (doi:10.1016/j.scriptamat.2011.04.023)
6. Xu W, Wang F, Ma D, Zhu X, Li D, Bührig-Polaczek A. 2020 Sliver defect formation in single crystal

Ni-based superalloy castings. *Mater. Des.* **196**. (doi:10.1016/j.matdes.2020.109138)

7. Huang Y, Shen J, Wang D, Xie G, Lu Y, Lou L, Zhang J. 2020 Formation of Sliver Defect in Ni-Based Single Crystal Superalloy. *Metall. Mater. Trans. A Phys. Metall. Mater. Sci.* **51**, 99–103. (doi:10.1007/s11661-019-05516-2)
8. Sanchez-Mata O, Wang X, Muñiz-Lerma JA, Atabay SE, Attarian Shandiz M, Brochu M. 2021 Dependence of mechanical properties on crystallographic orientation in nickel-based superalloy Hastelloy X fabricated by laser powder bed fusion. *J. Alloys Compd.* **865**, 158868. (doi:10.1016/j.jallcom.2021.158868)
9. Hallensleben P, Scholz F, Thome P, Schaar H, Steinbach I, Eggeler G, Frenzel J. 2019 On crystal mosaicity in single crystal Ni-based superalloys. *Crystals* **9**, 15–20. (doi:10.3390/cryst9030149)
10. Aveson JW *et al.* 2019 On the Deformation of Dendrites During Directional Solidification of a Nickel-Based Superalloy. *Metall. Mater. Trans. A Phys. Metall. Mater. Sci.* **50**, 5234–5241. (doi:10.1007/s11661-019-05429-0)
11. Hu S, Liu L, Yang W, Sun D, Huo M, Huang T, Zhang J, Su H, Fu H. 2019 Formation of Accumulated Misorientation During Directional Solidification of Ni-Based Single-Crystal Superalloys. *Metall. Mater. Trans. A Phys. Metall. Mater. Sci.* **50**, 1607–1610. (doi:10.1007/s11661-018-05109-5)
12. Sun D, Liu L, Yang W, Huang T, Huo M, Hu S, Zhang J, Fu H. 2019 Influence of Secondary Dendrite Orientation on the Evolution of Misorientation in the Platform Region of Single Crystal Superalloy Turbine Blades. *Adv. Eng. Mater.* **21**, 1–8. (doi:10.1002/adem.201800933)
13. Sun D, Liu L, Huang T, Yang W, Li Y, Yue Q, Zhang J, Fu H. 2018 Insight of the dendrite deformation in Ni-based superalloys for increased misorientation along convergent boundaries. *Prog. Nat. Sci. Mater. Int.* **28**, 489–495. (doi:10.1016/j.pnsc.2018.07.003)
14. Palumbo G, Piccininni A, Piglionico V, Guglielmi P, Sorgente D, Tricarico L. 2015 Modelling residual stresses in sand-cast superduplex stainless steel. *J. Mater. Process. Technol.* **217**, 253–261. (doi:10.1016/j.jmatprotec.2014.11.006)
15. Takaki T, Kashima H. 2011 Numerical investigations of stress in dendrites caused by gravity. *J. Cryst. Growth* **337**, 97–101. (doi:10.1016/j.jcrysgro.2011.10.012)
16. Srinivasan M, Karuppasamy P, Ramasamy P, Barua AK. 2016 Numerical modelling on stress and dislocation generation in multi-crystalline silicon during directional solidification for PV applications. *Electron. Mater. Lett.* **12**, 431–438. (doi:10.1007/s13391-016-4002-3)

17. Thorborg J, Klinkhammer J, Heitzer M. 2012 Transient and residual stresses in large castings, taking time effects into account. *IOP Conf. Ser. Mater. Sci. Eng.* **33**, 012050. (doi:10.1088/1757-899X/33/1/012050)
18. Fackeldey M, Ludwig A, Sahm PR. 2002 Coupled modelling of the solidification process predicting temperatures, stresses and microstructures. *Comput. Mater. Sci.* **7**, 194–199. (doi:10.1016/s0927-0256(96)00080-8)
19. Yamaguchi M, Beckermann C. 2013 Simulation of solid deformation during solidification: Shearing and compression of polycrystalline structures. *Acta Mater.* **61**, 2268–2280. (doi:10.1016/j.actamat.2012.12.047)
20. Yamaguchi M, Beckermann C. 2013 Simulation of solid deformation during solidification: Compression of a single dendrite. *Acta Mater.* **61**, 4053–4065. (doi:10.1016/j.actamat.2013.03.030)
21. Hu S, Yang W, Cui Q, Huang T, Zhang J, Liu L. 2017 Effect of secondary dendrite orientations on competitive growth of converging dendrites of Ni-based bi-crystal superalloys. *Mater. Charact.* **125**, 152–159. (doi:10.1016/j.matchar.2017.02.006)
22. Guo C, Takaki T, Sakane S, Ohno M, Shibuta Y, Mohri T. 2020 Overgrowth behavior at converging grain boundaries during competitive grain growth: A two-dimensional phase-field study. *Int. J. Heat Mass Transf.* **160**, 120196. (doi:10.1016/j.ijheatmasstransfer.2020.120196)
23. Xing H, Dong X, Wang J, Jin K. 2018 Orientation Dependence of Columnar Dendritic Growth with Sidebranching Behaviors in Directional Solidification: Insights from Phase-Field Simulations. *Metall. Mater. Trans. B Process Metall. Mater. Process. Sci.* **49**, 1547–1559. (doi:10.1007/s11663-018-1265-0)
24. Wang W, Lee PD, McLean M. 2003 A model of solidification microstructures in nickel-based superalloys: Predicting primary dendrite spacing selection. *Acta Mater.* **51**, 2971–2987. (doi:10.1016/S1359-6454(03)00110-1)
25. Lee PD, Atwood RC, Dashwood RJ, Nagaumi H. 2002 Modeling of porosity formation in direct chill cast aluminum-magnesium alloys. *Mater. Sci. Eng. A* **328**, 213–222. (doi:10.1016/S0921-5093(01)01687-2)
26. Lee PD, Chirazi A, Atwood RC, Wang W. 2004 Multiscale modelling of solidification microstructures, including microsegregation and microporosity, in an Al-Si-Cu alloy. *Mater. Sci. Eng. A* **365**, 57–65. (doi:10.1016/j.msea.2003.09.007)

27. Dong HB, Lee PD. 2005 Simulation of the columnar-to-equiaxed transition in directionally solidified Al-Cu alloys. *Acta Mater.* **53**, 659–668. (doi:10.1016/j.actamat.2004.10.019)

28. Kao A, Krastins I, Alexandrakis M, Shevchenko N, Eckert S, Pericleous K. 2019 A Parallel Cellular Automata Lattice Boltzmann Method for Convection-Driven Solidification. *Jom* **71**, 48–58. (doi:10.1007/s11837-018-3195-3)

29. Kao A, Shevchenko N, Alexandrakis M, Krastins I, Eckert S, Pericleous K. 2019 Thermal dependence of large-scale freckle defect formation. *Philos. Trans. R. Soc. A Math. Phys. Eng. Sci.* **377**, 20180206. (doi:10.1098/rsta.2018.0206)

30. Aveson JW, Reinhart G, Nguyen-Thi H, Mangelinck-Noël N, D'Souza N, Stone HJ. 2014 Origins of misorientation defects in single crystal castings: A time resolved in situ synchrotron X-ray radiography study. *MATEC Web Conf.* **14**. (doi:10.1051/matecconf/20141405003)

31. Slone AK, Pericleous K, Bailey C, Cross M, Bennett C. 2004 A finite volume unstructured mesh approach to dynamic fluid-structure interaction: An assessment of the challenge of predicting the onset of flutter. *Appl. Math. Model.* **28**, 211–239. (doi:10.1016/S0307-904X(03)00142-2)

32. Taylor GA, Bailey C, Cross M. 1995 Solution of the elastic/visco-plastic constitutive equations: A finite volume approach. *Appl. Math. Model.* **19**, 746–760. (doi:10.1016/0307-904X(95)00093-Y)

33. Oliveira PJ, Rente CJ. 1999 Development and Application of a Finite Volume Method for Static and Transient Stress Analysis. **1**, 297–309.

34. Uehara T, Fukui M, Ohno N. 2008 Phase field simulations of stress distributions in solidification structures. *J. Cryst. Growth* **310**, 1331–1336. (doi:10.1016/j.jcrysgro.2007.12.035)

35. Marcus Y. 2017 On the compressibility of liquid metals. *J. Chem. Thermodyn.* **109**, 11–15. (doi:10.1016/j.jct.2016.07.027)